




Article

Spray Cooling Investigation of TiO₂–Water Nanofluids on a Hot Surface

Yunus Tansu Aksoy , Hendrik Cornelissen, Pinar Eneren  and Maria Rosaria Vetrano * 

KU Leuven, Department of Mechanical Engineering, Division of Applied Mechanics and Energy Conversion (TME), B-3001 Leuven, Belgium; yunus.aksoy@kuleuven.be (Y.T.A.); pinar.eneren@kuleuven.be (P.E.)

* Correspondence: rosaria.vetrano@kuleuven.be

Abstract: Spray cooling is a heat transfer technology that has already shown its advantages and limitations. There has been increasing interest from academia and industry in combining this technology with nanofluids as coolants, owing to their potential for heat transfer enhancement. Nevertheless, there is a lack of understanding of the physical mechanism leading to this enhancement with the presence of technical problems that prevent the use of nanofluids in spray cooling applications. In this study, we investigate the effect of water-based TiO₂ nanofluids on both spray characteristics and heat transfer using an industrial full-cone pneumatic nozzle. For this purpose, three mass concentrations (0.05 wt.%, 0.1 wt.%, and 0.2 wt.%) were prepared and tested. We monitored the droplet sizes and velocity profiles with a particle dynamics analysis system. Moreover, the temporal temperature decrease of a heated aluminum block from 190 to 65 °C was measured via an infrared camera to calculate the heat transfer rate and heat transfer coefficient. The presence of nanoparticles is shown not to substantially alter the spray characteristics. Moreover, heat transfer is augmented mainly in the boiling regime due to more nucleation sites formed by the deposited nanoparticles. However, in the non-boiling regime, the contribution of adsorbed nanoparticles to the heat transfer enhancement diminishes. Overall, the aluminum block is cooled down 6%, 12%, and 25% faster than the DI water by the nanofluids at 0.05 wt.%, 0.1 wt.%, and 0.2 wt.%, respectively, including boiling and non-boiling regimes.

Keywords: spray cooling; nanofluid; heat transfer; nanoparticles



Citation: Aksoy, Y.T.; Cornelissen, H.; Eneren, P.; Vetrano, M.R. Spray Cooling Investigation of TiO₂–Water Nanofluids on a Hot Surface. *Energies* **2023**, *16*, 2938. <https://doi.org/10.3390/en16072938>

Academic Editor: Gabriela Humnic

Received: 23 February 2023

Revised: 16 March 2023

Accepted: 21 March 2023

Published: 23 March 2023



Copyright: © 2023 by the authors. Licensee MDPI, Basel, Switzerland. This article is an open access article distributed under the terms and conditions of the Creative Commons Attribution (CC BY) license (<https://creativecommons.org/licenses/by/4.0/>).

1. Introduction

Spray cooling is a widely used and high-efficient thermal management technique [1]. It can be defined as the process of forcing a liquid through a small orifice to atomize it into fine droplets, which are then directed to the target surface to be cooled [2]. Spray cooling is an important technology for many high-end industrial applications, such as microchip technology with limited room for heat sinks [3], supercomputers, e.g., Cray X-1 [4] or Dawning 5000A [5], quenching of hot metals in the metallurgical industry [6], and nuclear reactor containers requiring an excessive amount of heat removal [7,8]. Moreover, the miniaturized sizes of new-generation devices dissipate non-uniform heat fluxes that can locally exceed 1000 W/cm² [9]. Furthermore, sprays are applied in single-phase and boiling regimes to cool the electronics of hybrid vehicles, batteries, and LEDs [10,11]. Utmost attention should be placed on the thermal management of all heat-dissipating devices for better reliability, longer lifespans, and the maximum number of operation cycles [12]. To summarize, spray cooling enables high heat transfer rates and heat dissipation capacity at a low coolant flow rate, allowing for a more compact system design [13].

A spray cooling system can be configured by tuning several external parameters [14], e.g., the nozzle orifice diameter, flow rate, distance to the substrate, operating pressure, inlet temperature, and thermophysical properties of the coolant. Depending on a series of parameters of the liquid (boiling temperature, density, viscosity, surface tension), the spray

(droplets' velocity, size, and concentration), and the solid surface (material, temperature, roughness), a liquid film can form. This liquid may undergo a phase change and boil. Thus, to come up with heat transfer enhancement strategies, it is essential to understand the different heat transfer mechanisms, such as boiling on the wet surface, evaporation through the liquid film on the surface, and convective heat transfer [1,15]. Cooling solutions with extreme mass flow rates could be substituted by the use of nanofluids at lower mass flow rates to preserve energy and diminish the sizes of the cooling devices [16]. Nanofluids containing particles smaller than 100 nm are shown to have superior thermal properties than conventional coolants [17]. That is, the presence of these engineered nanoparticles in spray cooling would theoretically improve cooling performances with higher heat transfer rates.

Hsieh et al. [18] reported a substantial increase in both the convective heat transfer coefficient and critical heat flux, whereas Bellerova et al. [19,20] reported a detrimental effect of nanofluid spray on heat transfer. Figueiredo et al. [21] also observed a heat transfer enhancement with nanofluids compared to water owing to gold nanoparticles, yet some of this enhancement came from the surfactant addition via the increased wetting. Chang et al. [22] analyzed Al_2O_3 –water nanofluid sprays between 0.001 and 0.05 vol.% on copper surfaces with different surface roughness values and noticed the reduction in the convective heat transfer coefficient at higher nanoparticle concentrations caused by the particle deposition. According to Sanches et al. [23], nanoparticle shapes mildly modify the heat transfer coefficient and spray characteristics compared to the concentration effect. However, they claimed that it could be due to the nanoparticle deposition on the surface, whose impact on heat transfer is not yet clear. Indeed, on the one hand, it might create an insulation layer that deteriorates the heat removal capacity. On the other hand, it might increase surface roughness and facilitate the liquid to maintain a larger contact area with the surface [24]. Increased turbulence due to the boundary layer break-up by added nanoparticles might also be another possibility for altering the heat transfer characteristics [25]. Mitra et al. [26] saw an enhanced cooling rate with TiO_2 nanofluids in a laminar jet on a steel plate. Even though they also observed an earlier shift from the 'film boiling' to the 'transition boiling' regime with nanofluids, this shift might still be attributed to the vapor film instability of the nanoparticle deposition according to the order of magnitude analysis, not necessarily to the superior thermal properties. To conclude, most studies [27] agree on the improved nanofluid heat transfer in spray cooling, but there are some conflicting trends as well [19,23,25,28].

The role of nanoparticles in a single droplet that spreads and splashes is well documented and acts as a reasonable starting point for the spray phenomenon [29–32]. The changes in the droplet dynamics might explain the macroscopic effects on the spray characteristics, hence triggering different mechanisms for heat transfer enhancement [33]. According to Sanches et al. [23], the triangular shape of the nanoparticles adversely affects the heat transfer over spherical ones, especially at low-impact distances where the droplets have higher velocities and the heat transfer by convection is more sensitive due to increased viscosity. Since some rheological properties (density, viscosity, and surface tension) vary because of nanoparticle addition [18,34], the spray characteristics (velocity, droplet size, and cone angle) might also be influenced [35,36], thus modifying the heat transfer capabilities. Maly et al. [35] studied the impact of Al_2O_3 –water nanofluids on the spray characteristics in terms of their preparation methods and rheological properties. However, within the 0.5–2 wt.% concentration range, they observed a smaller spray cone angle and decreased diameter of the atomized droplets, but not more than the measurement uncertainty. On the contrary, Kang et al. [36] measured larger droplet sizes and smaller velocities with Al_2O_3 –water nanofluids between 0.2 and 0.5 wt.% compared to a water spray using a particle dynamics analyzer. Chang et al. [37] reported a lower heat transfer performance with a longer spray operation, which was presumably due to the gradual increase in the thickness of the nano-adsorption layer on the heated surface as measured

by scanning electron microscopy. To exploit the best nanofluids, smaller nanoparticles at lower concentrations are preferred to avoid clogging and material loss issues [38,39].

In this framework, our research investigates the droplet size and velocity, as well as the heat transfer of a nanofluid spray. First, we use a particle dynamics analysis (PDA) system to measure the nanofluid spray characteristics in terms of droplet velocity and size. Afterward, we measure the temperature changes in a heated aluminum block during the cooling process to calculate the heat removal from the surface by the spray at different nanoparticle concentrations.

2. Materials and Methods

2.1. Experimental Setup and Conditions

The experimental setup is presented in Figure 1. The ambient temperature T_{amb} and the relative humidity level were measured as 25 ± 1 °C and ≈ 40 %, respectively. The bulk liquids were stored at ambient temperatures in a reservoir of a 3 L pressure vessel. They were then pressurized using nitrogen gas and left to flow through a full cone nozzle with an orifice diameter of 0.6 mm and a spray cone angle of 60° . The pressure in the reservoir was fixed at 7 bar via a pressure regulation valve providing a constant flow rate of 3.12 L/h while the spray was in operation.

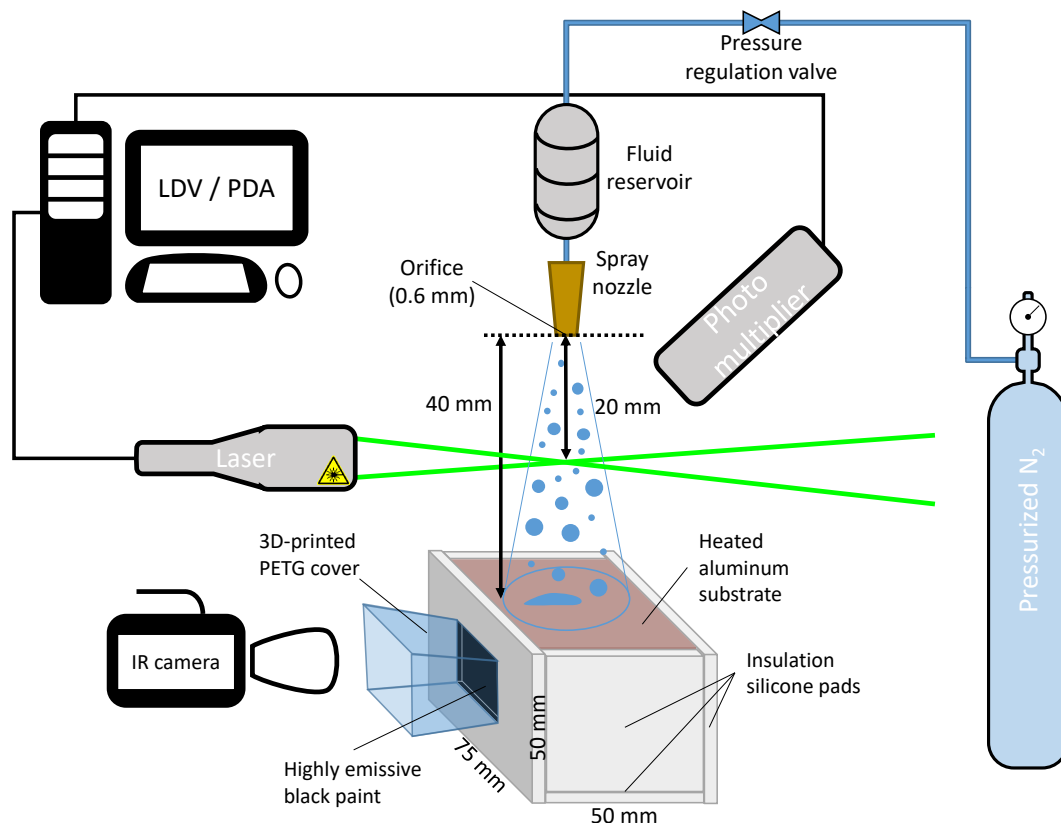


Figure 1. Experimental setup characterizing the nanofluid spray and measuring the temperature of the heated aluminum block.

2.1.1. Spray Characterization

The droplet velocity and size measurements were performed via the 1-D PDA system from Dantec Dynamics. The optical configuration is summarized in Table 1. Burst Spectrum Analyzer (BSA) flow software was used to control the experimental data acquisition with the following settings: a photomultiplier sensitivity of 1300 V, a signal gain of 12 dB, a velocity center of 17.5 m/s, and a velocity span of 35 m/s.

Table 1. Optical configuration of the Dantec Dynamics PDA system for the droplet size and velocity profiles.

Transmitting Optics		Receiving Optics	
Laser power	125 mW	Scattering angle	48°
Laser wavelength	532 nm	Receiver focal length	310 mm
Beam diameter	2.2 mm		
Beam spacing	36.91 mm		
Transmitter focal length	310 mm		
Frequency shift	40 MHz		

The PDA system creates a measurement volume by intersecting two laser beams that are located 20 mm below the spray nozzle (see Figure 1), where the spray is fully developed. The measurement points are defined at 7 equally spaced points in the radial direction, and the data acquisition is carried out by horizontally moving the spray by 3 mm at a time. In the PDA system, a mask allowing droplet sizes up to 113.8 μm is set, which is compatible with the droplets of the present spray. Using the phase plot in the BSA flow software, the sphericity of droplets is validated to be above 90%. The recording duration is limited to either the 10,000 acquired samples or a 30 s acquisition duration at each measurement point. The experiments were repeated at least three times to ensure repeatability.

Characteristic diameters better reflect the actual droplet size distribution across the spray since they consider the significance of larger droplets [35]. Plus, they may provide insight into the most appropriate spray characteristics that promote heat transfer. For instance, since high heat transfer rates occur along the three-phase contact line [40], bigger droplets result in a decreased heat transfer. Therefore, to represent the volume-to-surface area ratio, characteristic droplet sizes, e.g., the Sauter mean diameter (d_{32}), are statistically assessed from the sampled droplets and evaluated in Equation (1). It is expressed as a collection of spherical droplets of different diameters equal to the diameter of identical spherical droplets forming an equivalent collection of spheres [41].

$$d_{32} = \frac{\sum_{i=1}^N n_i d_i^3}{\sum_{i=1}^N n_i d_i^2} \quad (1)$$

To incorporate the uncertainty sources, such as pressure fluctuations, spray nozzle positioning, and the error in the PDA system itself, a standard deviation is calculated from the repeatability measurements with water [35], which is estimated to be less than 1.2 % for the d_{32} , and 1.1 % for the velocity. These small error bars are not displayed on the plots for the sake of clarity.

2.1.2. Evaluation of Heat Transfer

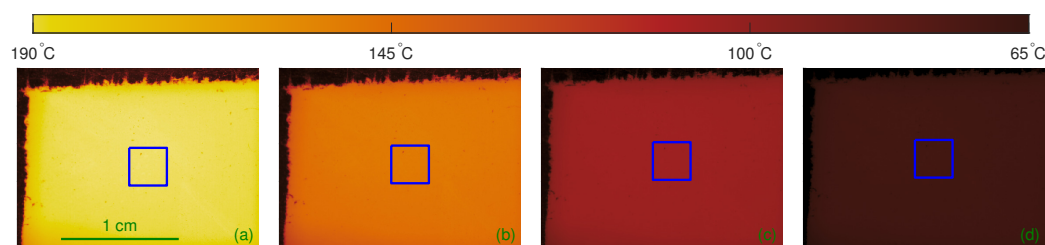
An aluminum (3003-H18) block with dimensions of $75 \times 50 \times 50 \text{ mm}^3$, a mass m_{Al} of 501.41 g, and a heat capacity C_{pAl} of 893 J/kg·K was used to test the cooling performances of the nanofluid sprays. The sides and the bottom of the aluminum block were insulated with 9 mm silicone pads to minimize the thermal losses to the surrounding (see Figure 1). A $30 \times 30 \text{ mm}^2$ area on one side of the aluminum block was painted with Sencys heat-resistant paint, whose color was a high-emissivity matte black for temperature field measurements. In particular, only the field of view of the infrared camera was painted to reduce radiative heat losses. Uniform cooling within the block was assumed owing to the high thermal conductivity of aluminum, i.e., 154 W/m·K.

The Optris PI 640 camera, whose specifications are summarized in Table 2, was employed for temperature measurements of the black-painted region of the aluminum block. An additional cover that was 3D-printed of PETG with a window was placed to prevent the field of view from being obstructed by the excess liquid from the top. This cover also helped to align the aluminum block to always be placed at the same location for experimental reproducibility.

Table 2. Specifications of the Optris PI 640 infrared camera.

	System Accuracy	Thermal Sensitivity	Optical Resolution	Frame Rate	Spatial Resolution
Optris PI 640	$\pm 2\text{ }^{\circ}\text{C}$	75 mK	$640 \times 480\text{ px}^2$	32 fps	$32\text{ }\mu\text{m/px}$

For each experiment, the aluminum block was heated at a temperature of over $190\text{ }^{\circ}\text{C}$ and placed 40 mm below the spray nozzle at a fixed location. The spray was simultaneously operated with the infrared camera until the aluminum block was cooled down below $65\text{ }^{\circ}\text{C}$. A 2D temperature field was obtained via the infrared camera software. Some examples of the raw images are reported in Figure 2. Out of the uniform temperature fields, a window of $100 \times 100\text{ px}^2$ was selected (blue squares), and the average temporal temperature profile was used for further analysis. To lower the measurement noise and uncertainty, the data were downsampled to 1 Hz during post-processing without causing any impact on the temperature profiles.

**Figure 2.** Examples of raw infrared camera images during the spray cooling process at different temperatures: (a) $190\text{ }^{\circ}\text{C}$, (b) $145\text{ }^{\circ}\text{C}$, (c) $100\text{ }^{\circ}\text{C}$, and (d) $65\text{ }^{\circ}\text{C}$. The same magnification factor applies to all images.

2.2. Nanofluid Preparation

Three different mass concentrations of nanofluids ($C_w = 0.05\text{ wt.}\%$, $0.1\text{ wt.}\%$, and $0.2\text{ wt.}\%$) were prepared from a stable and well-dispersed commercial water-based TiO_2 nanofluid (rutile, 40 wt.%, 30–50 nm size range, Io-li-tec Ionic Liquids Technologies GmbH). Only deionized (DI) water was added during dilution (neither dispersants nor surfactants). To ensure good mixing, the diluted nanofluids were subjected to a vortex mixer and a sonic bath. After that, the median diameters were verified via the light extinction spectroscopy LES technique [42,43], as well as the stability and dispersity of the nanofluids. The measured particle size distribution and the corresponding log-normal fit are illustrated in Figure 3. The fit on the LES data shows a median diameter of 70.1 nm and a non-dimensional dispersity level (coefficient of variation) of 0.3. Moreover, the same LES results were achieved after 2 h, proving the temporal stability of the nanofluids and the absence of particle clustering formation.

The experimental characterization of all the samples in terms of the density ρ , surface tension σ , and viscosity η , are detailed in [29] and listed in Table 3. Briefly, a pycnometer (BlauBrand, Gay–Lussac pattern, calibrated, 10.109 mL), ARES-G2 rheometer (TA instruments, a double-walled Couette cell at shear rates between 1 and 200 s^{-1}), and an optical tensiometer (Biolin Scientific Theta Lite, 5 drops, 60 images per drop at 2 fps, Young–Laplace fit) are employed for density, viscosity, and surface tension measurements, respectively.

Slight differences among those properties are not expected to affect the spray characteristics. Further, no significant increase in thermal conductivity is anticipated due to the low concentration of TiO_2 nanoparticles based on correlations summarized in [27].

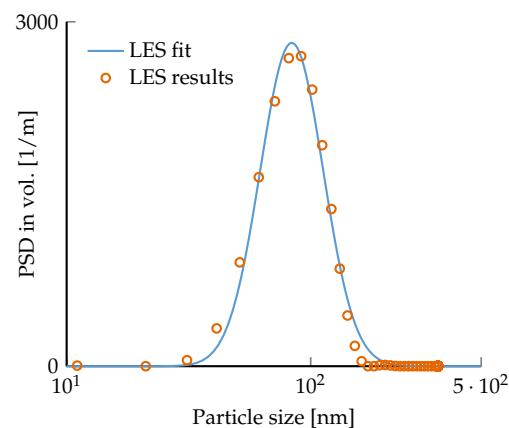


Figure 3. Particle size distribution of TiO₂–water nanofluid at 0.2 wt.% measured by the LES technique. A log-normal fit of the experimental results gives the median diameter of 70.1 nm with a non-dimensional dispersity level of 0.3.

Table 3. Measured rheological properties of the water and water-based TiO₂ nanofluids.

	C_w [%]	ρ $\left[\frac{\text{kg}}{\text{m}^3}\right]$	σ $\left[\frac{\text{mN}}{\text{m}}\right]$	η [mPa·s]
Water	0	996.00	71.0	1.00
TiO ₂ –water	0.05	996.29	70.3	1.00
TiO ₂ –water	0.1	996.47	69.4	1.01
TiO ₂ –water	0.2	996.80	68.9	1.02

3. Results and Discussions

3.1. Effect of Nanoparticles on Droplet Size and Velocity Profiles

In Figure 4a, the Sauter mean diameter d_{32} for the sprays of DI water and two nanoparticle concentrations (0.1 wt.% and 0.2 wt.%) are plotted along the radial direction, demonstrating the experimental repeatability. It should be noted that further concentrations, such as 0.33 wt.%, cause nozzle clogging. As the x-axis represents the radial direction, the size distribution of the spray droplets can be seen at 7 measurement points with the middle one as the origin, i.e., the location of the spray orifice axis. The radial evolution of d_{32} follows what is expected and observed in the literature. On the spray orifice axis, the d_{32} is smaller due to gas entrainment, which carries the smaller droplets owing to their higher sensitivity to the drag force [44,45]. The d_{32} gradually increases while moving away from the center toward the edge of the spray. Although the size profile of the spray slightly deviates from the symmetry, this deviation stays within the uncertainty of the horizontal position. However, the difference from the symmetry diminishes toward the edge of the spray. The same d_{32} evolution along the radial direction is observed despite different TiO₂ nanoparticle concentrations, which do not alter the spray characteristics in terms of the d_{32} . This is similar to the results by Kang et al. [36] with Al₂O₃ nanofluids up to 0.4 wt.%. However, they report considerably larger diameters, especially at the center of the spray, for an Al₂O₃ nanofluid concentration of 0.5 wt.%. If the average droplet diameters are taken into account (see Figure 4b), a positive trend of increasing the nanoparticle concentration is observed within the measurement uncertainties. This might imply a reduction in the spray performance due to nanoparticles but the deviation is below 1.4%. Higher viscosity due to the presence of nanoparticles might also have a negative impact while the bulk liquid is disintegrated during the atomization [36].

Parallel to the size comparison, droplet velocity profiles of DI water and nanofluids in the radial direction are plotted in Figure 4c. A cone shape with the highest velocities at the center, gradually decreasing toward the edge, represents a typical droplet velocity profile for all fluids. This profile is also complementary to the droplet size measurements:

small droplets possess the highest speeds at the center and vice versa. There exists a slight negative trend in the velocity by increased nanoparticle concentration, similar to the observations in [35,36,46]. According to the results presented in this section, water-based TiO_2 nanofluids at low concentrations do not substantially modify the spray characteristics under the same conditions.

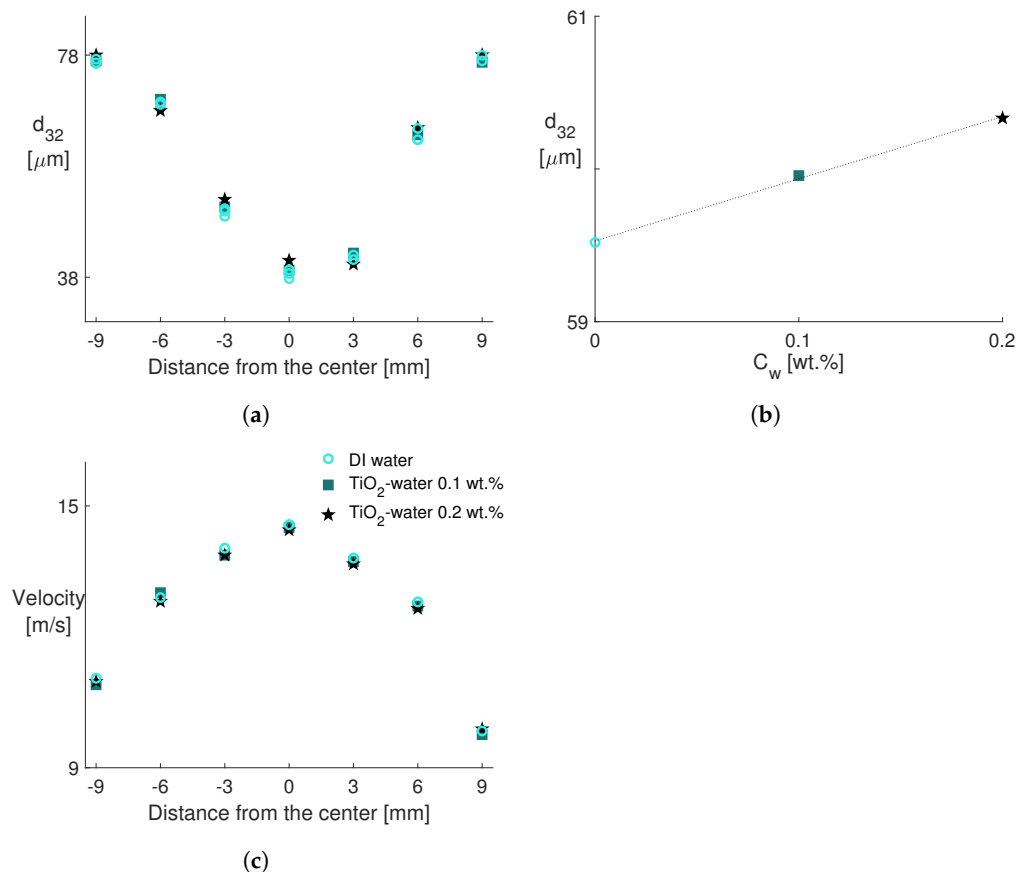


Figure 4. Effect of the nanoparticle concentration on (a) d_{32} profile along the radial direction (with 3 types of repeatability test data for DI water), (b) averaged d_{32} along the radial direction as a function of C_w , and (c) velocity profiles. The same legend applies to all plots.

3.2. Effect of Nanoparticles on Heat Transfer

This section discusses the heat transfer improvement under the spray conditions applied in the previous section (e.g., injection pressure, ambient temperature, etc.). Temperature measurements are conducted with each fluid at least three times to confirm the experimental repeatability. For example, Figure 5a illustrates the temporal decrease in the average temperature of the aluminum block $T_{Al}(t)$ from 190 to 65 °C for DI water. The plot shows remarkable repeatability of the temperature decrease during the tests and includes their averages. Since the nanofluids exhibit the same behavior, the corresponding average temperature decrease is considered in the following analyses. Figure 5b compares the temporal decrease in the temperature of the aluminum block using the spray from DI water and water-based nanofluids, in which the shaded areas along the curves represent the measurement uncertainties. The elapsed time for the aluminum block temperature to decrease from 190 to 65 °C clearly decreases with the increasing nanoparticle concentration. Above the saturation temperature of DI water, nanofluid at a 0.2 wt.% concentration demonstrates faster cooling.

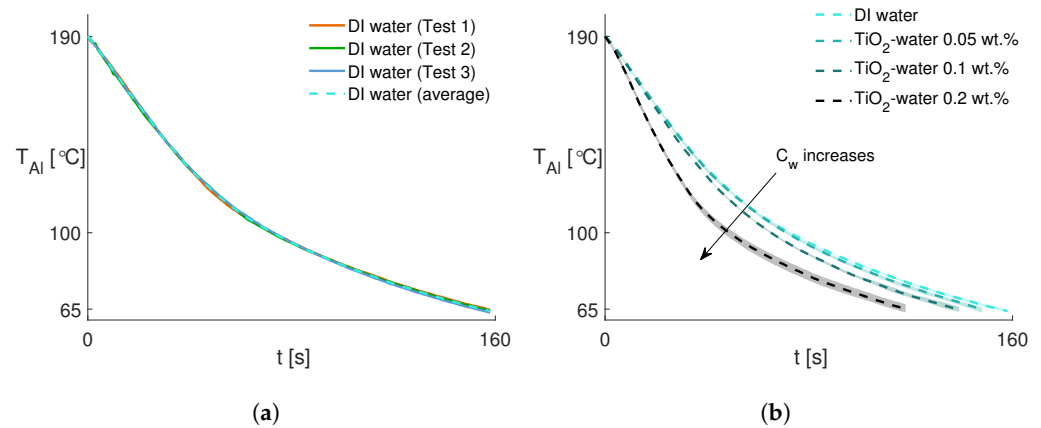


Figure 5. (a) Temperature drops in the aluminum block over time for DI water as a repeatability check, including the average profile (dashed line). (b) Comparison of the temperature drops in the aluminum block over time for each fluid with uncertainty (shaded areas).

One of the reasons for the observed cooling enhancement might be the improved thermal properties of the nanofluids [47], i.e., higher thermal conductivity k and thermal diffusivity $k/(\rho C_p)$. However, it is not expected that thermal conductivity will increase by more than 1% at low TiO_2 nanoparticle loadings [48,49], which means that other mechanisms should be considered to explain this heat transfer enhancement. Another explanation could be the surface modification due to nanoparticles. Although the mechanism of the nanoparticle deposition on the surface is not yet totally described, the surface coating by nanoparticles [50] would either promote or prevent heat transfer [23]. During spray cooling with nanofluids, nanoparticles may accumulate on the surface and form a rough layer, especially at high temperatures when the liquid film on the hot surface undergoes complete evaporation. If the nanoparticles possess a relatively lower thermal conductivity than the heated surface, the formed layer may act as an insulator and deteriorate the heat transfer process. However, if the nanoparticles have comparable thermal conductivity, their deposition would enlarge the surface area and increase the number of nucleation sites in the boiling regime by forming irregular shapes. As a consequence, enrichment in heat transfer would be acquired. In the case under investigation, the thermal conductivity of TiO_2 nanoparticles and the inevitable oxidation layer of Al_2O_3 on the aluminum surface [51] are of the same order of magnitude. Consequently, the particle deposition might be the reason for the strong heat transfer enhancement.

Next, the heat transfer rate Q from the aluminum block to the fluid during the cooling process is calculated with Equation (2). The term $\frac{\Delta T}{\Delta t}$ is computed by the central finite difference formula, as given in Equation (3), where Δt is the time difference between each consecutive but downsampled infrared camera image and $T_{Al}(t)$ is the temperature of the aluminum block at the corresponding instant t .

$$Q = m_{Al} C_{p,Al} \frac{\Delta T}{\Delta t} \quad (2)$$

$$\frac{\Delta T}{\Delta t} = \frac{T_{Al}(t + \Delta t) - T_{Al}(t - \Delta t)}{2\Delta t} \quad (3)$$

The heat transfer rate as a function of time is presented in Figure 6a. The solid lines in the inset depict the whole cooling process of the aluminum block for each fluid. The markers show a range in which the temperature of the aluminum block is higher than 100 °C and their colors indicate the temperature. We consider that range as the boiling regime, whereas the temperature lower than 100 °C is addressed as the non-boiling regime.

In addition, the temporal evolution of the heat transfer coefficient of the spray $h(t)$ (see Equation (4)) is plotted in Figure 6b to complement the heat transfer rate.

$$h(t) = \frac{Q(t)}{A_{Al}(T_{Al}(t) - T_f)} \quad (4)$$

where T_f is the constant fluid temperature (25 °C) and A_{Al} is the top surface area of the aluminum block. In Figure 6, there is a period of a few seconds, during which the heat transfer rate and the heat transfer coefficients are almost constant and followed by a rapid increase for all fluids for ≈ 10 s. To further elaborate, in the first few seconds, at high temperatures, most of the droplets evaporate immediately even before reaching the hot surface. Consequently, only the nanoparticles hit the solid surface. Then, as the air above the surface contains more water vapor, the droplet evaporation decreases and the droplets start to impact the surface with a resultant strong increase in the heat transfer process. As the aluminum block cools down, a thin liquid film begins to accumulate near the edges of the surface, where the spray droplet concentration is weaker. In the middle, it is impossible to confirm the presence of the film due to the high droplet concentration, thus preventing any optical access. In the boiling regime, we observe an increase in heat transfer as a function of the nanoparticle concentration, which can be related to the nanoparticle deposition phenomenon, as mentioned earlier. This improvement is clearer in the heat transfer coefficient since it also incorporates the temperature difference between the surface and the fluid. The least nanoparticle concentration, i.e., 0.05 wt.%, does not demonstrate any appreciable increase in the heat transfer rate, probably due to the fast flow of the spray. A slight increase in heat transfer occurs at the concentration of 0.1 wt.% appearing as a bumpy pattern, which could be ascribed to two phenomena. The first possibility may be the non-uniform nanoparticle deposition on the surface due to the uneven distribution within the spray droplets, which induces localized regions with enhanced nucleation sites. As the first regions are suppressed by the increasing thickness of the nanoparticle layer acting as insulation, new ones are formed, giving rise to the peaks. The second possibility is that these peaks could correspond to an initial deposition of nanoparticles, which is then flushed away by the liquid film flowing on the surface. A further increase in the nanoparticle concentration to 0.2 wt.% provides continuous deposition and nucleation sites on the surface, leading to a drastic jump in heat transfer. This might be due to the formation of nanoparticle agglomerates during droplet evaporation while approaching the hot surface. Since these agglomerates become larger and heavier, their flushing may be impeded. Nonetheless, this heat transfer enhancement cannot be sustained in the non-boiling regime as it is convection-dominated and there is no more need for nucleation sites. Only the increased heat flux area contributes to heat transfer for a few degrees after the boiling finishes, which can be seen in the first half of the non-boiling regime in the inset of Figure 6b. Further, the heat transfer coefficient of the spray remains invariant with nanoparticle concentration in the second half of the non-boiling regime.

The heat E removed from the aluminum block by the spray is evaluated in Equation (5), where the heat transfer rate $Q(t)$ in Equation (2) is integrated over a time interval that covers the temperature decrease from 190 to 65 °C. Accordingly, Figure 7a shows the transferred energy as a function of time. The nanoparticle concentration effect, already evidenced in Figure 5b, is observed more clearly in Figure 7a. The elapsed time to extract the same energy from the aluminum block during the cooling process is then correlated to the nanoparticle concentration and the expected decreasing trend is shown in Figure 7b. The higher the nanoparticle concentration, the more energy is taken from the aluminum block. The nanofluids with increasing nanoparticle concentrations cool the aluminum block faster than the DI water by 6%, 12%, and 25%, respectively, considering the combined effects in both boiling and non-boiling regimes.

$$E = \int Q(t) dt \quad (5)$$

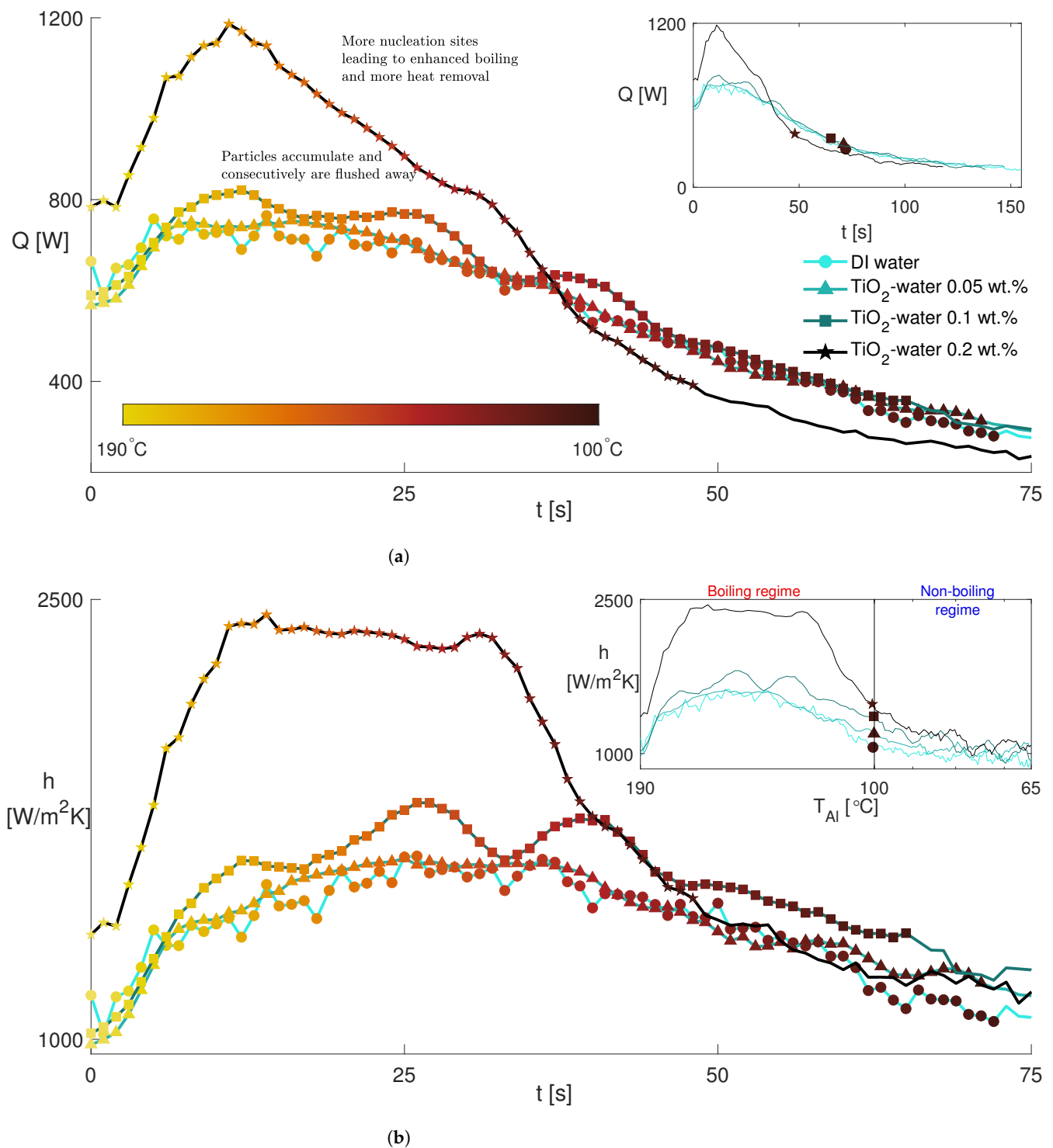


Figure 6. (a) Heat transfer rate from the aluminum block to the spray as a function of time. (b) Temporal evolution of the heat transfer coefficient of the spray. Both insets display the whole cooling process from 190 to 65 °C, whereas only the boiling regime is expressed in the main figures. To give insight into the cooling process, a temperature colormap is applied to the markers to highlight the boiling regime (190 °C and 100 °C). The same legend applies to all figures.

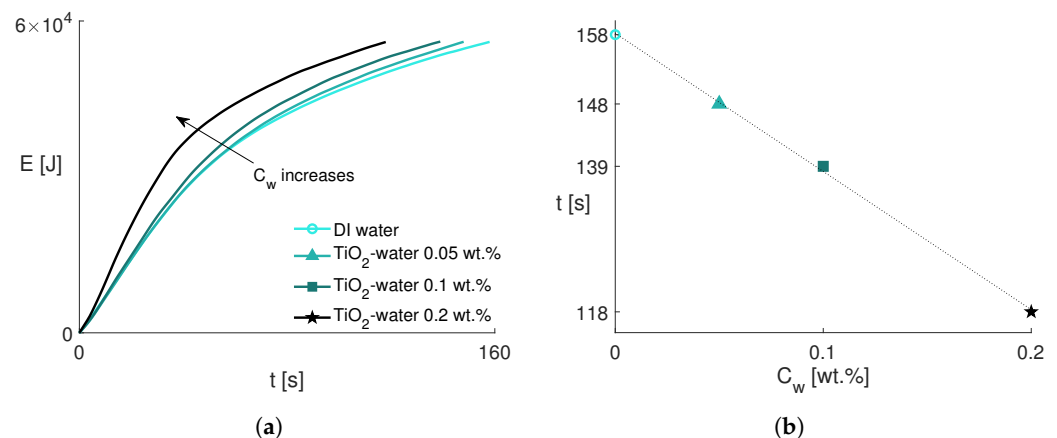


Figure 7. (a) Energy removed from the aluminum block as a function of time. (b) Elapsed time to extract the same energy from the aluminum block to cool it down from 190 to 65 °C as a function of nanofluid concentration. The same legend applies to both figures.

4. Conclusions and Perspectives

This experimental work examines the impact of water-based TiO_2 nanofluids on spray dynamics and heat transfer. Three different nanofluids at 0.05 wt.%, 0.1 wt.%, and 0.2 wt.% concentrations were prepared in DI water with ensured stability and well-dispersity. The spray characteristics are represented in terms of the Sauter mean diameters and droplet velocities. Heat transfer improvement was evaluated through temperature measurements on a heated aluminum block.

Typical droplet size and velocity profiles in the radial direction are obtained for DI water and water-based TiO_2 nanofluids: smaller droplets having high speeds at the center and gradually larger droplets with lower speeds toward the edge. A marginal increase in the average droplet size with increasing nanoparticle concentration reveals that the presence of the nanoparticles does not affect atomization, i.e., no change in the spray characteristics. However, a further increase in the nanoparticle concentration (e.g., 0.33 wt.%) results in clogging in the spray nozzle.

To compare the heat transfer performance, the temperature reduction from 190 to 65 °C of the aluminum block is monitored with an infrared camera as a function of time. The overall temperature drop, which includes both boiling and non-boiling regimes, shows a reduction in the cooling time with the increasing nanoparticle concentration. More specifically, the nanofluids at 0.05 wt.%, 0.1 wt.%, and 0.2 wt.% cool the aluminum block faster than the DI water by 6%, 12%, and 25%, respectively. This heat transfer enhancement cannot be justified by the marginal change in the thermal conductivity due to the nanoparticle addition, but by several phenomena: an augmented number of nucleation sites due to nanoparticle adsorption on the surface, non-uniform nanoparticle deposition, and partial flushing of the nanoparticles from the surface. For the nanofluid at 0.05 wt.%, heat transfer enhancement is minimal since the particles cannot adsorb on the surface of the aluminum block due to the high flow of the spray. With an increase in the nanoparticle concentration to 0.1 wt.%, a bumpy pattern of the heat transfer coefficient is observed over time. The peaks in the heat transfer curve correspond to the deposited particles, which are then flushed away, giving a decline to the heat transfer. At the highest concentration before clogging, i.e., 0.2 wt.%, a drastic increase is obtained during which the nanoparticles adsorb on the surface, giving rise to the nucleation sites and heat flux area. After the boiling is concluded, the heat transfer enhancement gradually diminishes since there is no need for nucleation sites.

Although there is a heat transfer increase by the use of nanofluids, their potential is limited due to clogging in the nozzle that arises from high particle concentrations. Further research to link nanofluids and the atomization process would provide physical insight to overcome this problem. The understanding of the interaction between the heated surface and the nanoparticles requires the evolution of the liquid film thickness during different

boiling regimes and the analyses of the surface morphology before, during, and after the cooling process. Surface roughness tests, polarization resistance measurements, and electrochemical impedance spectroscopy would provide information about the modification characteristics. Moreover, the monitoring of the evaporation rate of nanofluid droplets before the impact on the liquid film is essential to understand the possible formation of dry nanoparticle agglomerates and their mixing into the film.

Author Contributions: Conceptualization, Y.T.A.; methodology, Y.T.A. and H.C.; software, Y.T.A. and H.C.; validation, Y.T.A. and P.E.; formal analysis, Y.T.A., P.E. and H.C.; investigation, H.C.; resources, M.R.V.; data curation, Y.T.A. and H.C.; writing—original draft preparation, Y.T.A., P.E. and M.R.V.; writing—review and editing, Y.T.A., P.E. and M.R.V.; visualization, Y.T.A. and P.E.; supervision, P.E. and M.R.V.; project administration, Y.T.A. and M.R.V.; funding acquisition, M.R.V. All authors have read and agreed to the published version of the manuscript.

Funding: This research was financially supported by the Interne Fondsen KU Leuven/Internal Funds KU Leuven (C24/18/057 and C3/21/029).

Data Availability Statement: The data that support the findings of this study are available from the corresponding author upon reasonable request.

Acknowledgments: The authors thank Eleonora Ferraris for her generous support with the infrared camera. The authors also gratefully acknowledge the in-kind support of the Department of Chemical Engineering, KU Leuven with the nanofluid characterization devices.

Conflicts of Interest: The authors declare no conflict of interest. The funders had no role in the design of the study; in the collection, analyses, or interpretation of data; in the writing of the manuscript; or in the decision to publish the results.

Abbreviations

LES	Light Extinction Spectroscopy
PDA	Particle Dynamics Analysis
BSA	Burst Spectrum Analyzer

References

1. Yin, J.; Wang, S.; Sang, X.; Zhou, Z.; Chen, B.; Thrassos, P.; Romeos, A.; Giannadakis, A. Spray Cooling as a High-Efficient Thermal Management Solution: A Review. *Energies* **2022**, *15*, 8547. [\[CrossRef\]](#)
2. Xie, J.; Gan, Z.; Duan, F.; Wong, T.; Yu, S.; Zhao, R. Characterization of spray atomization and heat transfer of pressure swirl nozzles. *Int. J. Therm. Sci.* **2013**, *68*, 94–102. [\[CrossRef\]](#)
3. Smakulski, P.; Pietrowicz, S. A review of the capabilities of high heat flux removal by porous materials, microchannels and spray cooling techniques. *Appl. Therm. Eng.* **2016**, *104*, 636–646. [\[CrossRef\]](#)
4. Kim, J. Spray cooling heat transfer: The state of the art. *Int. J. Heat Fluid Flow* **2007**, *28*, 753–767. [\[CrossRef\]](#)
5. Chen, H.; long Cheng, W.; wei Zhang, W.; hang Peng, Y.; jia Jiang, L. Energy saving evaluation of a novel energy system based on spray cooling for supercomputer center. *Energy* **2017**, *141*, 304–315. [\[CrossRef\]](#)
6. Anisiuba, V.; Ma, H.; Silaen, A.; Zhou, C. Computational Studies of Air-Mist Spray Cooling in Continuous Casting. *Energies* **2021**, *14*, 7339. [\[CrossRef\]](#)
7. Sagawa, N. An Experimental Study of Spray Cooling in Nuclear Reactor Containers. *J. Nucl. Sci. Technol.* **1968**, *5*, 419–426. [\[CrossRef\]](#)
8. Zhang, H.; Ma, Y.; Hu, G.; Liu, Q. Droplet impaction in nuclear installations and safety analysis: Phenomena, findings and approaches. *Nucl. Eng. Des.* **2020**, *366*, 110757. [\[CrossRef\]](#)
9. Gatapova, E.Y.; Sahu, G.; Khandekar, S.; Hu, R. Thermal management of high-power LED module with single-phase liquid jet array. *Appl. Therm. Eng.* **2021**, *184*, 116270. [\[CrossRef\]](#)
10. Liang, G.; Mudawar, I. Review of spray cooling—Part 1: Single-phase and nucleate boiling regimes, and critical heat flux. *Int. J. Heat Mass Transf.* **2017**, *115*, 1174–1205. [\[CrossRef\]](#)
11. Liang, G.; Mudawar, I. Review of spray cooling—Part 2: High temperature boiling regimes and quenching applications. *Int. J. Heat Mass Transf.* **2017**, *115*, 1206–1222. [\[CrossRef\]](#)
12. Devahdhanush, V.; Mudawar, I. Review of Critical Heat Flux (CHF) in Jet Impingement Boiling. *Int. J. Heat Mass Transf.* **2021**, *169*, 120893. [\[CrossRef\]](#)
13. Xie, J.; Tan, Y.; Duan, F.; Ranjith, K.; Wong, T.; Toh, K.; Choo, K.; Chan, P. Study of heat transfer enhancement for structured surfaces in spray cooling. *Appl. Therm. Eng.* **2013**, *59*, 464–472. [\[CrossRef\]](#)

14. Khandekar, S.; Jaiswal, A.K.; Sahu, G. Chapter Four—Spray Cooling: From Droplet Dynamics to System Level Perspectives. In *Advances in Heat Transfer*; Elsevier: Amsterdam, The Netherlands, 2022; Volume 54, pp. 135–177. [\[CrossRef\]](#)
15. Zhang, T.; Mo, Z.; Xu, X.; Liu, X.; Chen, H.; Han, Z.; Yan, Y.; Jin, Y. Advanced Study of Spray Cooling: From Theories to Applications. *Energies* **2022**, *15*, 9219. [\[CrossRef\]](#)
16. Moita, A.; Moreira, A.; Pereira, J. Nanofluids for the Next Generation Thermal Management of Electronics: A Review. *Symmetry* **2021**, *13*, 1362. [\[CrossRef\]](#)
17. Choi, S.U.; Eastman, J.A. Enhancing thermal conductivity of fluids with nanoparticles. In Proceedings of the ASME International Mechanical Engineering Congress and Exposition, San Francisco, CA, USA, 12–17 November 1995.
18. Hsieh, S.S.; Liu, H.H.; Yeh, Y.F. Nanofluids spray heat transfer enhancement. *Int. J. Heat Mass Transf.* **2016**, *94*, 104–118. [\[CrossRef\]](#)
19. Bellerova, H.; Tseng, A.A.; Pohanka, M.; Raudensky, M. Spray cooling by solid jet nozzles using alumina/water nanofluids. *Int. J. Therm. Sci.* **2012**, *62*, 127–137. [\[CrossRef\]](#)
20. Bellerova, H.; Tseng, A.A.; Pohanka, M.; Raudensky, M. Heat transfer of spray cooling using alumina/water nanofluids with full cone nozzles. *Heat Mass Transf.* **2012**, *48*, 1971–1983. [\[CrossRef\]](#)
21. Figueiredo, M.; Marseglia, G.; Moita, A.S.; Panão, M.R.O.; Ribeiro, A.P.C.; Medaglia, C.M.; Moreira, A.L.N. Thermofluid Characterization of Nanofluid Spray Cooling Combining Phase Doppler Interferometry with High-Speed Visualization and Time-Resolved IR Thermography. *Energies* **2020**, *13*, 5864. [\[CrossRef\]](#)
22. Chang, T.B.; Syu, S.C.; Yang, Y.K. Effects of particle volume fraction on spray heat transfer performance of Al₂O₃-water nanofluid. *Int. J. Heat Mass Transf.* **2012**, *55*, 1014–1021. [\[CrossRef\]](#)
23. Sanches, M.; Marseglia, G.; Ribeiro, A.P.C.; Moreira, A.L.N.; Moita, A.S. Nanofluids Characterization for Spray Cooling Applications. *Symmetry* **2021**, *13*, 788. [\[CrossRef\]](#)
24. Bai, P.; Zhou, L.; Huang, X.; Du, X. How wettability affects boiling heat transfer: A three-dimensional analysis with surface potential energy. *Int. J. Heat Mass Transf.* **2021**, *175*, 121391. [\[CrossRef\]](#)
25. Hsieh, S.S.; Leu, H.Y.; Liu, H.H. Spray cooling characteristics of nanofluids for electronic power devices. *Nanoscale Res. Lett.* **2015**, *10*, 139. [\[CrossRef\]](#) [\[PubMed\]](#)
26. Mitra, S.; Saha, S.K.; Chakraborty, S.; Das, S. Study on boiling heat transfer of water-TiO₂ and water-MWCNT nanofluids based laminar jet impingement on heated steel surface. *Appl. Therm. Eng.* **2012**, *37*, 353–359. [\[CrossRef\]](#)
27. Aksoy, Y.T.; Zhu, Y.; Eneren, P.; Koos, E.; Vetrano, M.R. The Impact of Nanofluids on Droplet/Spray Cooling of a Heated Surface: A Critical Review. *Energies* **2021**, *14*, 80. [\[CrossRef\]](#)
28. Tseng, A.A.; Bellerova, H.; Pohanka, M.; Raudensky, M. Effects of Titania nanoparticles on heat transfer performance of spray cooling with full cone nozzle. *Appl. Therm. Eng.* **2014**, *62*, 20–27. [\[CrossRef\]](#)
29. Aksoy, Y.; Eneren, P.; Koos, E.; Vetrano, M. Spreading-splashing transition of nanofluid droplets on a smooth flat surface. *J. Colloid Interface Sci.* **2022**, *606*, 434–443. [\[CrossRef\]](#)
30. Aksoy, Y.T.; Liu, L.; Abboud, M.; Vetrano, M.R.; Koos, E. Role of Nanoparticles in Nanofluid Droplet Impact on Solid Surfaces. *Langmuir* **2023**, *39*, 12–19. [\[CrossRef\]](#)
31. Aksoy, Y.T.; Eneren, P.; Koos, E.; Vetrano, M.R. Spreading of a droplet impacting on a smooth flat surface: How liquid viscosity influences the maximum spreading time and spreading ratio. *Phys. Fluids* **2022**, *34*, 042106. [\[CrossRef\]](#)
32. Aksoy, Y.T.; Eneren, P.; Koos, E.; Vetrano, M.R. Spreading Dynamics of Al₂O₃-water Nanofluid Droplets Impacting On a Smooth Flat Surface. In Proceedings of the 7th World Congress on Momentum, Heat and Mass Transfer (MHMT'22), Virtual, 7–9 April 2022. [\[CrossRef\]](#)
33. Aksoy, Y. How Nanofluids Influence Droplet Impact on a Solid Substrate and Surface-to-Droplet Heat Transfer. Ph.D. Thesis, KU Leuven, Leuven, Belgium, 2022.
34. Estelle, P.; Cabaleiro, D.; Zyla, G.; Lugo, L.; Murshed, S.S. Current trends in surface tension and wetting behavior of nanofluids. *Renew. Sustain. Energy Rev.* **2018**, *94*, 931–944. [\[CrossRef\]](#)
35. Maly, M.; Moita, A.S.; Jedelsky, J.; Ribeiro, A.P.C.; Moreira, A.L.N. Effect of nanoparticles concentration on the characteristics of nanofluid sprays for cooling applications. *J. Therm. Anal. Calorim.* **2019**, *135*, 3375–3386. [\[CrossRef\]](#)
36. Kang, B.; Marengo, M.; Begg, S. A Study of the Effect of Nanoparticle Concentration on the Characteristics of Nanofluid Sprays. *J. Appl. Fluid Mech.* **2019**, *12*, 413–420. [\[CrossRef\]](#)
37. Chang, T.B.; Lin, T.H.; Huang, J.W. Experimental investigation into spray cooling heat transfer performance of Al₂O₃-water nanofluid with different subcooling degrees. *Proc. Inst. Mech. Eng. Part E J. Process. Mech. Eng.* **2022**, *236*, 245–253. [\[CrossRef\]](#)
38. Eneren, P.; Aksoy, Y.T.; Vetrano, M.R. Experiments on Single-Phase Nanofluid Heat Transfer Mechanisms in Microchannel Heat Sinks: A Review. *Energies* **2022**, *15*, 2525. [\[CrossRef\]](#)
39. Eneren, P. The Impact of Nanofluids on Single-Phase Convective Heat Transfer in Microchannels. Ph.D. Thesis, KU Leuven, Leuven, Belgium, 2022.
40. Guggilla, G.; Narayanaswamy, R.; Pattamatta, A. An experimental investigation into the spread and heat transfer dynamics of a train of two concentric impinging droplets over a heated surface. *Exp. Therm. Fluid Sci.* **2020**, *110*, 109916. [\[CrossRef\]](#)
41. Kowalczyk, P.B.; Drzymala, J. Physical meaning of the Sauter mean diameter of spherical particulate matter. *Part. Sci. Technol.* **2016**, *34*, 645–647. [\[CrossRef\]](#)
42. Eneren, P.; Aksoy, Y.T.; Zhu, Y.; Koos, E.; Vetrano, M.R. Light extinction spectroscopy applied to polystyrene colloids: Sensitivity to complex refractive index uncertainties and to noise. *J. Quant. Spectrosc. Radiat. Transf.* **2021**, *261*, 107494. [\[CrossRef\]](#)

43. Horváth, I.; Colinet, P.; Vetrano, M. Assessment of the light extinction spectroscopy technique for submicron particle characterization. *Powder Technol.* **2016**, *291*, 375–382. [[CrossRef](#)]
44. Cossali, G.E. An integral model for gas entrainment into full cone sprays. *J. Fluid Mech.* **2001**, *439*, 353–366. [[CrossRef](#)]
45. Foissac, A.; Malet, J.; Vetrano, M.R.; Buchlin, J.M.; Mimouni, S.; Feuillebois, F.; Simonin, O. Droplet size and velocity measurements at the outlet of a hollow cone spray nozzle. *At. Sprays* **2011**, *21*, 893–905. [[CrossRef](#)]
46. Kannaiyan, K.; Sadr, R. The effects of alumina nanoparticles as fuel additives on the spray characteristics of gas-to-liquid jet fuels. *Exp. Therm. Fluid Sci.* **2017**, *87*, 93–103. [[CrossRef](#)]
47. Apmann, K.; Fulmer, R.; Soto, A.; Vafaei, S. Thermal Conductivity and Viscosity: Review and Optimization of Effects of Nanoparticles. *Materials* **2021**, *14*, 1291. [[CrossRef](#)] [[PubMed](#)]
48. Batmunkh, M.; Tanshen, M.R.; Nine, M.J.; Myekhlai, M.; Choi, H.; Chung, H.; Jeong, H. Thermal Conductivity of TiO₂ Nanoparticles Based Aqueous Nanofluids with an Addition of a Modified Silver Particle. *Ind. Eng. Chem. Res.* **2014**, *53*, 8445–8451. [[CrossRef](#)]
49. Wanatasanapan, V.; Abdullah, M.; Gunnasegaran, P. Effect of TiO₂-Al₂O₃ nanoparticle mixing ratio on the thermal conductivity, rheological properties, and dynamic viscosity of water-based hybrid nanofluid. *J. Mater. Res. Technol.* **2020**, *9*, 13781–13792. [[CrossRef](#)]
50. Hedge, R.; Rao, S.; Reddy, R. Flow visualization and study of CHF enhancement in pool boiling with Al₂O₃—Water nano-fluids. *Therm. Sci.* **2012**, *16*, 445–453. [[CrossRef](#)]
51. Nguyen, L.; Hashimoto, T.; Zakharov, D.N.; Stach, E.A.; Rooney, A.P.; Berkels, B.; Thompson, G.E.; Haigh, S.J.; Burnett, T.L. Atomic-Scale Insights into the Oxidation of Aluminum. *ACS Appl. Mater. Interfaces* **2018**, *10*, 2230–2235. [[CrossRef](#)] [[PubMed](#)]

Disclaimer/Publisher's Note: The statements, opinions and data contained in all publications are solely those of the individual author(s) and contributor(s) and not of MDPI and/or the editor(s). MDPI and/or the editor(s) disclaim responsibility for any injury to people or property resulting from any ideas, methods, instructions or products referred to in the content.